Proceedings of ASME Turbo Expo 2011
GT2011
June 6-10, 2011, Vancouver, British Columbia, Canada

GT2011-45883

TIME-RESOLVED NUMERICAL INVESTIGATION OF THE INTERACTION OF LABYRINTH SEAL LEAKAGE AND MAIN-FLOW IN A 1.5-STAGE LP TURBINE

Marc H.-O. Biester, Lasse Mueller, Joerg R. Seume
Institute of Turbomachinery and Fluid Dynamics
Leibniz Universitaet Hannover
Appelstr. 9, 30167 Hannover, Germany
Email: biester@tfd.uni-hannover.de

Yavuz Guendogdu
MTU Aero Engines GmbH & Co.KG
Dachauer Str. 665
80995 München, Germany

ABSTRACT

In axial turbomachinery such as low pressure turbines, shrouded airfoils with labyrinth seals are commonly used. Among different sealing options, labyrinth seals in particular are characterized by long term durability and high sealing efficiency. Since a leakage flow is inevitable, a thorough understanding of how the leakage flow exits the cavities, its interaction with the main flow, and the induction of losses is necessary. In order to take into account unsteady effects, three-dimensional time resolved RANS computations of a 1.5 stage LPT rig in its design operating point are conducted. To capture effects in the boundary layer, a low Reynolds approach is used at the blade surface as well as on the hub and tip surfaces. To match the real geometry of the turbine blades, fillets have been modeled. Simulations were performed using the TRACE solver developed by the German Aerospace Center (DLR). The investigation shows how cavity flows have a significant influence on the main-flow aerodynamics and the loss generation. Steady and unsteady results with full spatially discretized cavities show a significant decrease of isentropic efficiency compared to simulations without cavities. The efficiency drop for the steady and time-averaged cavity computations can be explained with intensified secondary flow. The time resolved calculation shows a strong non-uniformity of the leakage flux depending on the instantaneous circumferential position of the up- and downstream blades. The time dependent ingress of cavity leakage results in the formation of a counter-rotating vortex pair. In terms of the influence on the main flow, it is shown that the interaction is limited to the end walls with almost no influence on the midspan flow.

NOMENCLATURE

c	=	Chord length
h	=	Blade height
$\dot{m}$	=	Mass flow
N	=	Blade count
n	=	Rotational speed
p	=	Pressure
r	=	Stage reaction
s	=	Entropy
t	=	Pitch
T	=	Temperature
$\underline{u}$	=	Velocity vector

Subscripts

ax	=	Axial
E	=	Turbine entry
is	=	Isentropic
l	=	Leakage
p	=	Constant pressure process
ref	=	Reference
stg	=	Stage
t	=	Total
Θ	=	Tangential component
v	=	Constant volume process

Greek symbols

α	=	Yaw angle
β	=	Stagger angle
η	=	Efficiency

Π	=	Pressure ratio
ρ	=	Density
ϕ	=	Flow coefficient
ψ	=	Stage loading coefficient
Ω	=	Vorticity

Abbreviation

LE	=	Leading edge
LPT	=	Low pressure turbine
PS	=	Pressure side
SS	=	Suction side
TE	=	Trailing edge
Re	=	Reynolds number
RPM	=	Revolutions per minute

INTRODUCTION

In axial turbomachinery such as low pressure turbines, shrouded airfoils with labyrinth seals are commonly used. Among different sealing options, labyrinth seals in particular are characterized by long term durability and high sealing efficiency. Furthermore, compared to unshrouded airfoils, this sealing arrangement reduces secondary flow in the blade row and corresponding losses since the tip vortex can be avoided. Most numerical analysis still assume a smooth end wall surface without axial gaps, cavities, and seals due to the vast additional effort the discretization of cavities require. This simplification leads to a significant difference between computational and experimental results. In conjunction with the presence of time-dependent effects as, among others, described by Pfau et al. [1] further time resolved investigation is necessary.

Denton and Johnson [2] initially investigated labyrinth leakage jet behavior. They show that the leakage flow experiences almost no deflection when bypassing the airfoil. As a consequence, while re-entering the main flow, mixing losses occur due to the difference in momentum and flow direction of the leakage and main flow resulting in an increase in entropy. Denton [3] gives a theory to quantify the amount of entropy generation by this mechanism. A reduction can be attained by reducing the deviation of the tangential velocity of main and leakage flow. Based on these findings, several attempts have been made. Wallis et al. [4] found that a decrease in loss can be achieved by redirecting the leakage flow and point out the importance of understanding unsteady and three dimensional flow phenomena which occur in the shroud region with regard to the success of the device used for the turning of the leakage flow. Rosic and Denton [5] demonstrate that it is possible to improve the flow field in the subsequent blade row by reducing the aerodynamic mixing loss in circumferential direction. They also state that the effectiveness of the turning vanes depends on their geometry and vane-to-vane spacing. A more detailed view of the significant

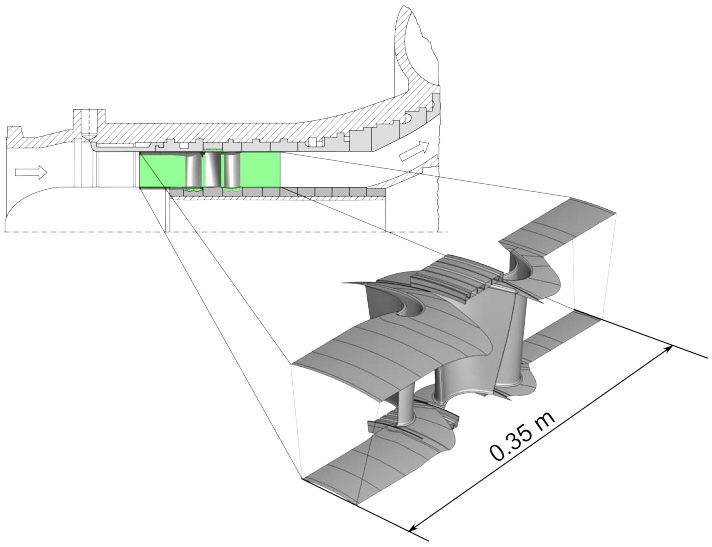

FIGURE 1: COMPUTATED REGION OF THE TURBINE

loss mechanisms is given by Wallis et al. [4]. The analysis reveals that the majority of the losses are due to mixing in the labyrinth chambers downstream of each fin, bypass, mixing, and the non-ideal incidence on the downstream blade row whereas loss caused by windage is fairly negligible. Gier et al. [6] confirm these mechanisms and attempt to separate and quantify them. Anker and Mayer [7] point out that due to the non-ideal incidence separation and consequently increased loss can be observed. However, the principle of a labyrinth seal is the dissipation of kinetic energy to minimize the fraction of leakage. Therefore, the most promising way to achieve reduction of aerodynamic losses is the minimization of entropy generation when re-entering the main flow.

Nevertheless, losses are not only generated in close vicinity to the cavity's outlet but also far more downstream. As a consequence of the relative motion between the end walls of stationary and rotating frame, the boundary layer of the non deflected near wall fluid is skewed as, among others, described by Hunter and Manwaring [8], Boletis et al. [9] and Walsh and Gregory-Smith [10]. The shearing amplifies all characteristic features associated with the usual end wall vortex system and therefore enhances the formation of secondary flow structures within the flow field. The sheared boundary layer and passage vortex have the same sense of rotation what results in an enlargement of the latter. Bindon [11] confirms the increase of the passage vortex caused by leakage flow and describes why lossy fluid of the end wall regions moves to midspan regions. Boletis et al. [9] specify the mechanism of this movement.

TABLE 1: OPERATIONAL DATA AND BLADE CHARACTERISTICS

Rotational speed n [min^{-1}]	7000		
Inlet pressure $p_{t,E}$ [kPa]	156.7		
Inlet temperature $T_{t,E}$ [K]	370		
Mass flow $\dot{m}_E$ [kg/s]	8.5		
Stage pressure ratio Π_{stg} [-]	1.43		
Net power [kW]	278		
	Stator 1	Rotor	Stator 2
Number of blades N [-]	18	30	36
h/c_{ax} [-]	2.15	2.15	2.15
t/c [-]	0.986	0.729	0.722
β_s [$^\circ$]	39.08	51.21	67.98
Flow coefficient ϕ [-]	-	0.59	-
Stage loading coefficient ψ [-]	1.95		-
Stage reaction r [-]	0.55		-
Reynolds number $Re \cdot 10^5$ [-]	7.54	6.48	4.17

In recent years, further experimental and numerical investigations concerning the interaction of the main and cavity flow have been conducted. Pfau et al. [12] carry out experimental analysis in a turbine cascade and in a 2-stage turbine engine (see [13] and [1]). It is revealed that due to the difference in static pressure at suction and pressure side of the blade a strong circumferential dependency of the flow field in the cavity can be detected, as also shown in the work of Wallis et al. [4]. Numerical studies of the labyrinth clearance height is conducted by Anker and Mayer [14], [7]. They approve the increase of secondary flow formation in regions downstream of the cavity outlet and found that for moderate radial clearance the leakage flow leaves the main flow on the pressure side and re-enters on the suction side for cavity in- and outlet. The latter is also responsible for further vortex generation.

TEST RIG

Figure 1 shows a longitudinal half-section of the turbine and indicates the simulated region. The blade characteristics of the LPT and stage parameters are listed in Tab. 1. A detailed view of the MTU designed blade geometry is given in Fig. 2. Figure 3 shows the detailed geometry of the labyrinth seals, the axial extension of the cavity in- and outlet, and the radial gap between

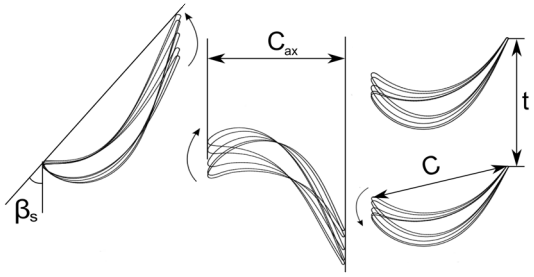

FIGURE 2: DETAILED BLADE VIEW

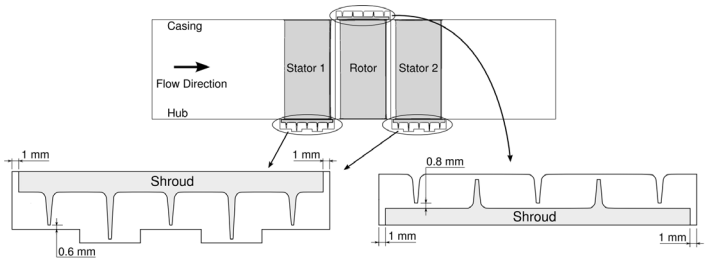

FIGURE 3: CAVITY GEOMETRY

TABLE 2: CAVITY LEAKAGE FLOW FOR STEADY AND TIME-RESOLVED CALCULATIONS

Cavity leakage	Stator 1	Rotor	Stator 2
$\frac{\dot{m}_l}{\dot{m}_E}$ [%] (steady)	0.423	0.888	0.240
$\frac{\dot{m}_l}{\dot{m}_E}$ [%] (unsteady)	0.419	0.889	0.242

seal fin and casing. Each labyrinth consists of five seal fins. The resulting leakage flow determined by the steady and unsteady computation is listed in Tab. 2 related to the turbine inlet mass flow $\dot{m}_E$.

NUMERICAL METHODS

Simulations are performed using a parallel Unsteady Reynolds-Averaged Navier Stokes (URANS) flow solver for structured and unstructured grids referred to as TRACE (Turbomachinery Research Aerodynamics Computational Environment). TRACE is developed by the Institute of Propulsion Technology of the German Aerospace Center (DLR) in cooperation with MTU Aero Engines to model and investigate turbomachinery flow. The RANS closure problem is dissolved by using the Wilcox k-ω turbulence model (see Wilcox [15]) in a low Reynolds version with a fix of the turbulent production term in k by Kato and Launder (Kožulović et al. [16]) and extensions for

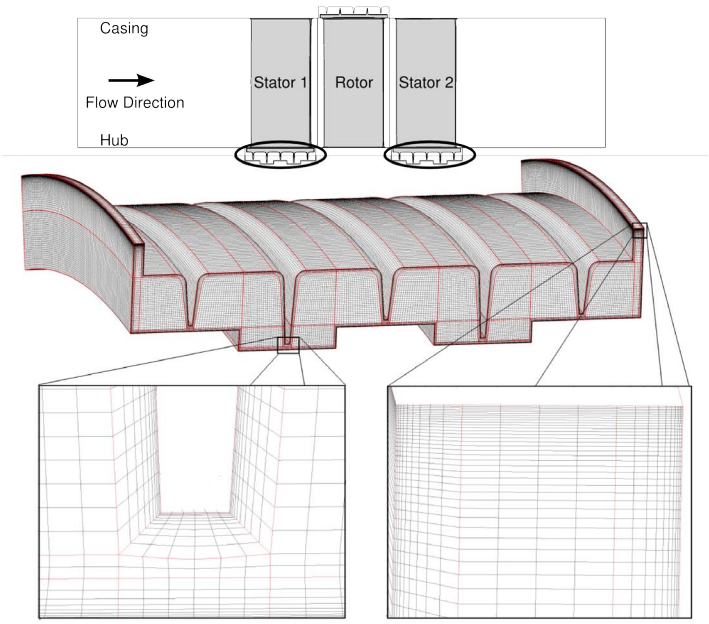

FIGURE 4: MESH OF THE FIRST AND SECOND STATOR LABYRINTH SEAL

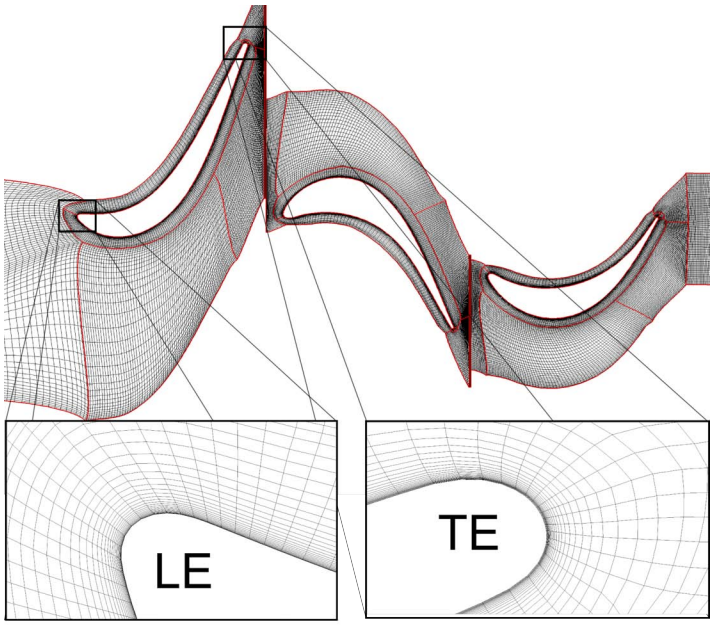

FIGURE 5: COMPUTATIONAL GRID AT MIDSPAN. DETAIL VIEW OF VANE 1 LE AND TE

system rotation. According to Wilcox [17], the k-ω turbulence model as used in this calculations is able to predict laminar to turbulent transition. However, it can be shown that these predictions generally are not entirely accurate. Thus, a correlation-based multimode transition model is employed (see Kožulović et al. [18]) to describe boundary layer pattern, which has been calibrated to provide good results of natural, bypass, separation, and wake induced transition. Spatial discretization for flux calculation is realized by using an upwind-based total variation diminishing (TVD) scheme by Roe with a van Leer MUSCLE extrapolation to attain second order accuracy. To avoid numerical oscillation, e.g. in case of shock, a Van Albada flux limiter is used. For the steady-state simulation, temporal discretization is achieved by a first order implicit Euler backward scheme. For the transient simulation, an implicit second order Euler backward scheme is employed. Inter-row coupling for stationary frame calculations is achieved by using a mixing plane method, for time resolved calculations a conservative zonal approach based on flux interpolation with second order accuracy is used which adapts the inter-row boundary conditions to match the rotation. The mesh itself is not moved. The interfaces between stationary and rotating frame are located at approximately 10% axial chord-length downstream of the stator or rotor, respectively. Cavity coupling is realized by a conservative mixed cell approach as described by Yang et al. [19]. The location of the cavity in- and outlet relative to the inter-row interfaces varies for rotor and stator. The distance between the outlet of the first stator cavity and the downstream interface equals approximately 2.5% axial chord length while the distance between the outlet of the rotor cavity and interface amounts approximately 1.25% axial chord length .

Mesh

Considered flow passes the stages in an annular channel of constant radius at hub and shroud. Non-cylindrical parts of the turbine are excluded to diminish the need for computational resources (see Fig. 1). In order to capture the real geometry of the turbine blades and, as pointed out by Kuegeler et al. [20], to improve the quality of the prediction, fillets have been modeled. In respect of in-boundary layer effects and to obtain a highly resolved flow field, a low Reynolds approach is used at the airfoil and end wall regions as well as within the cavities. Transition modeling as described above is only applied at the airfoil suction side. The necessary y^+ value of $y^+ \approx 1$ in combination with Reynolds numbers around 500.000 and a maximum stretching ratio of 1.2 of adjacent near wall cells results in a vast increase in nodes (see detailed view in Fig. 5). In preparation of this work, a grid sensitivity study based on a quasi three-dimensional mesh of regarded turbine has been performed for steady state calculations which shows that for further refinement nearly no substantial improvement can be gained while for a coarsened mesh changes in the result are not negligible. Fig. 5 shows the used H-O-C-G-block topology which is uniform for all blades and gives an idea of the mesh density. Regarding the cavity mesh, similar attempts have been made concerning the

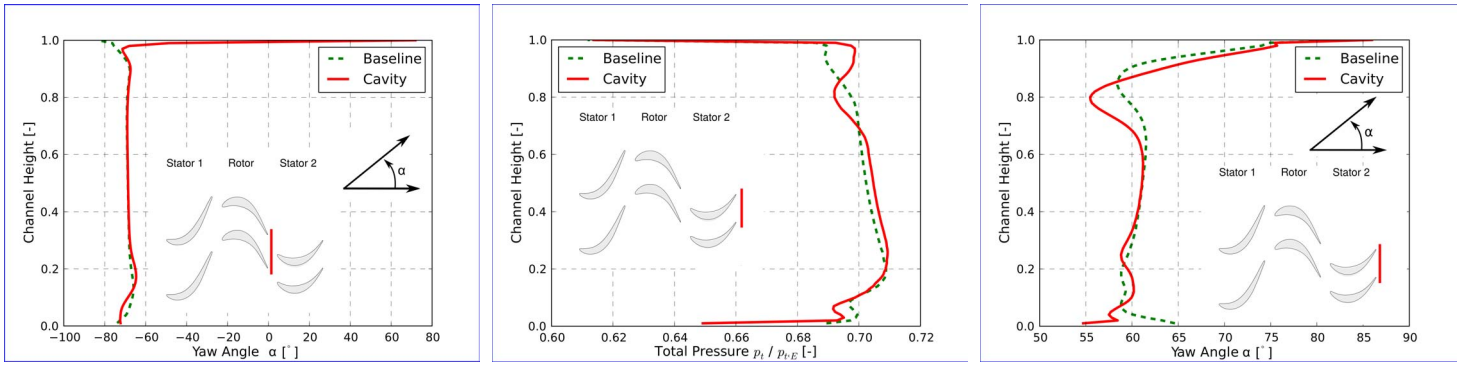

(a) (b) (c)

FIGURE 6: CIRCUMFERENTIALLY AVERAGED DISTRIBUTION OF: (a) YAW ANGLE BEHIND ROTOR (RELATIVE FRAME), (b) TOTAL PRESSURE BEHIND STATOR 2 , (c) YAW ANGLE BEHIND STATOR 2

mesh density and cell distribution. To match the experimental periodicity, the simulation of three vanes, five blades, and six vanes (each equal to 60° cutout) for transient calculations is mandatory. This leads to a structured mesh of 51,846,536 nodes for the time resolved calculations; no unstructured elements are used.

The structured mesh discretizing the cavities is shown in Fig. 4. In order to maintain uniformity with the mesh of the main flow, structured hexahedral elements are used. To guarantee a smooth junction between the in- and outlet of the cavity, refinement in this region matches the cell width in the end wall regions as shown in the right detailed view in Fig. 4. Furthermore, the same requirements like stretch ratio etc. are satisfied.

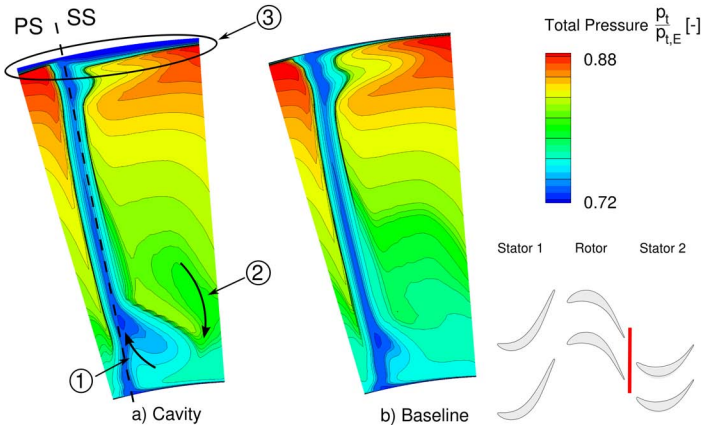

FIGURE 7: STAGNATION PRESSURE BEHIND ROTOR

STEADY STATE RESULTS

In conducted steady-state simulations inter-row coupling has been achieved by using a mixing-plane approach, i.e. due to the pitch-wise averaging unsteady effects like wakes are mixed out. This obvious disadvantage regarding the influence of unsteady effects onto the development of the flow structure is opposed by the fact that the impact of local disturbance such as labyrinth leakage on the flow field can be identified without a superposition of vortex structures generated in upstream blade rows. To analyze the phenomena induced by leakage flow, two planes located at approximately 10% axial chord length behind the regarded blade have been selected for evaluation, located upstream of each mixing plane.

Figure 7 shows the distribution of the stagnation pressure p_t normalized with the total pressure at turbine entry $p_{t,E}$ behind the rotor (as additionally indicated in Fig. 7) for the simulation with cavities (*a*) and the simulation with a smooth and uninterrupted end wall (*b*) looking in upstream direction. The leakage flow of the rotor cavity has a lower level of total pressure and re-enters the main flow directly upstream of the evaluated plane (③ in Fig. 7). Due to the difference in pressure on the suction and pressure side of the blade, the distribution of the leakage flow varies with the circumferential position i.e. in the vicinity of the suction side the quantity of leakage flow is significantly higher than near the pressure side. This non-uniform distribution is enhanced by unsteady effects as shown later. Furthermore, Fig. 7 exhibits the existence of a passage vortex (as indicated by arrows) on the hub and tip side. Comparison of both simulations reveals an intensification of this vortex due to the cavity flow of the first stator cavity. On the suction side this leads to a relocation of low momentum fluid up to 25% span ①.

In return, on the pressure side fluid of high momentum is lifted to the hub ②. The maximum drop in total pressure due to the intensified secondary flow can be found at 20% span.

Fig. 6a shows the pitch-wise and mass flow averaged distribution of the yaw angle behind the rotor (in the relative frame). Corresponding to the sense of rotation of the passage vortex as sketched in Fig. 7, the main flow is overturned up to approximately 10% span and underturned from 10% to 25% span. Furthermore, it can be confirmed that, as described by Denton and Johnson [2], the cavity leakage experiences almost no deflection since the flow angle of the fluid decreases down to 75° starting at approximately 95% channel height. This is the amount of the flow angle downstream of the first stator row and leads to a very strong negative incidence on the second stator row. A similar flow field can be identified behind the second stator.

Fig. 6b shows the circumferentially and mass flow averaged distribution of the total pressure behind the second stator normalized with the total pressure at turbine entry $p_{t,E}$. The fluctuation in the vicinity of the tip exhibits a passage vortex with its core at approximately 85% span. This can be confirmed by the circumferentially and mass flow averaged yaw angle as depicted in Fig. 6c. Within the region from 20% to 70% span the stagnation pressure is slightly higher than in the simulation without cavities. This increase is due to the displacement of the main flow caused by the reinforced secondary flow and following blockage. The amplified and reduced deflection extends from 60% to 100% span. In the vicinity of the hub the cavity leakage can be indicated easily in Fig. 6c as there is almost no deflection within the cavity.

Loss Generation

Previous section introduces the mechanism by which the labyrinth leakage flow is affecting the formation of secondary flow. To identify regions of loss generation due to leakage ingress, which is according do Denton [3] equal to an increase in entropy, evaluation of the entropy within the flow field is carried out for both simulations. Presuming a perfect gas, the specific entropy can be calculated as

$$\Delta s = c_v \ln\left(\frac{p}{p_{ref}}\right) + c_p \ln\left(\frac{\rho_{ref}}{\rho}\right). \qquad (1)$$

Figure 8 shows the mass flow averaged specific entropy evolution defined by Eq. 1 through the turbine for simulations with cavities (*Cavity*) as well as without them (*Baseline*). In order to indicate the axial position of entropy generation, a meridional view of the turbine is sketched in Fig. 8. Losses which are generated in the cavities are not taken into account

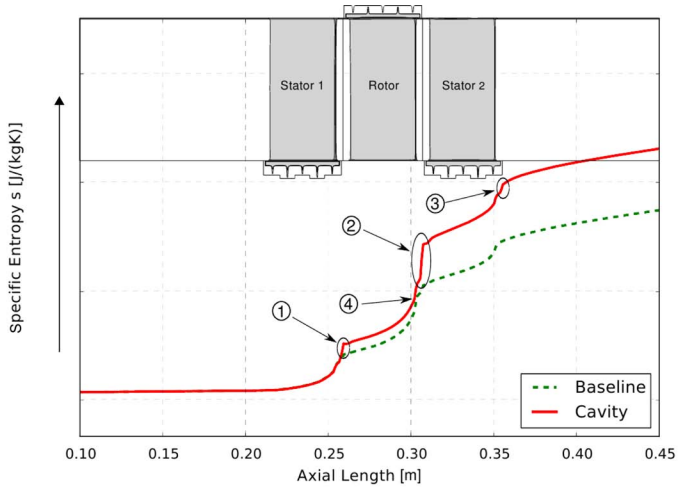

FIGURE 8: ENTROPY DISTRIBUTION IN THE TURBINE WITH (CAVITY) AND WITHOUT CAVITIES (BASELINE)

until the leakage flow is re-entering the main flow. The ingress of rotor cavity leakage-flow heads to a very strong and steep gain of entropy (② in Fig. 8) whereas leakage flow of the stator cavities leads to a moderate swell of losses (① and ③ in Fig. 8). The difference in entropy generation between the blade rows can be tracked down to two effects. The first is due to the bigger leakage flow of the rotor cavity. Since the functional principle of a labyrinth seal is dissipation of kinetic energy, the flow field within the cavities is strongly three dimensional, dominated by vortices, and involves heavy losses. However, this cannot culminate in the observed increase. As pointed out by Denton [3], entropy generation in mixing processes depends on the rate of shear strain and thus it is a function of the flow angle at in- and outlet. Since the rotor blade causes the highest flow deflection, the maximum of entropy generation is at the outlet of the rotor cavity. Another remarkable characteristic is the growth of entropy within the blade rows. As shown in Fig. 8, for the configuration with cavities the increase of entropy in the rotor is less intense than in the configuration without them, what causes both distributions to meet in ④.

A more detailed view of the loss generation within the blade rows is given in Fig. 9a and Fig. 9b which depict the mass flow weighted circumferentially averaged total-to-total isentropic efficiency in the stationary frame drawn over the channel height. Reference for the inlet conditions is the turbine inlet. The analyzed plane is positioned at 10% axial chord length downstream of the blade. Therefore, the evaluated volume covers the first stage (Fig. 9a) and the whole 1.5 stage turbine (Fig. 9b), respectively. Figure 9a indicates a clear difference at the hub up to 30% channel height between both configurations. Thus, loss generation in this area due to the leakage flow of the first stator cavity

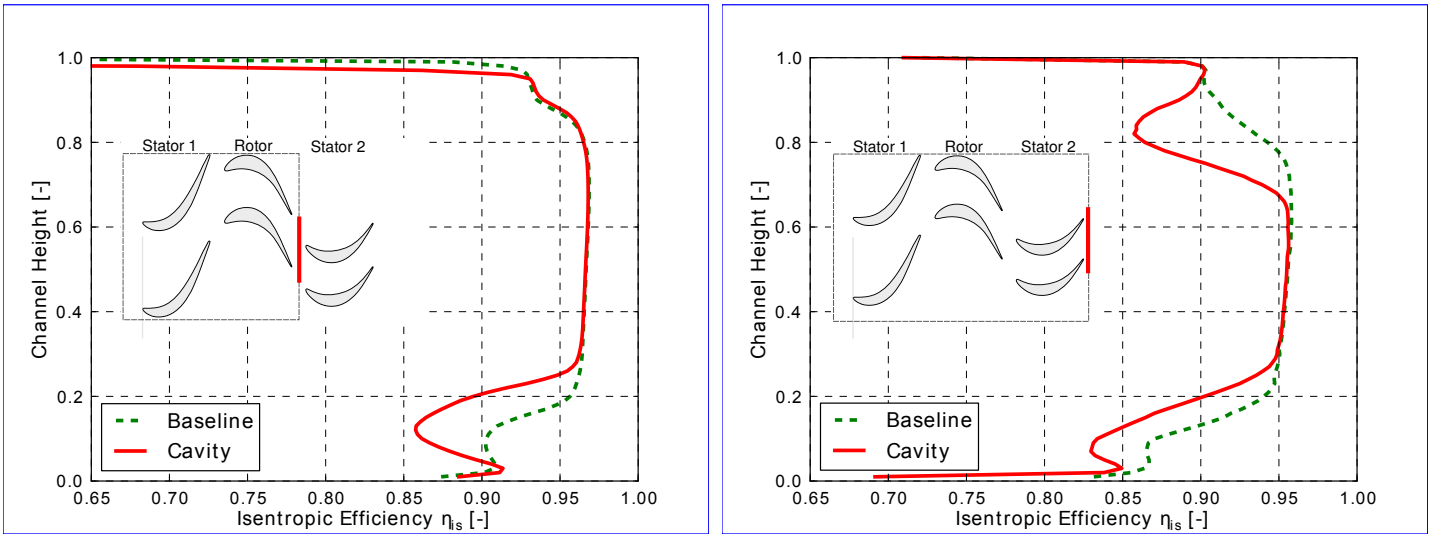

FIGURE 9: CIRCUMFERENTIALLY AVERAGED DISTRIBUTION OF: (a) ISENTROPIC EFFICIENCY OF FIRST STAGE, (b) ISENTROPIC EFFICIENCY OF TURBINE

and resulting grow of secondary flow in the rotor passage can clearly be identified. From 30% to 85% channel height no discrepancy between both patterns is detectable as the isentropic efficiency remains constant at $\eta_{is} \approx 97\%$. In the vicinity of the tip a strong decay of isentropic efficiency down to 10% occurs. This is caused by the ingress of the rotor cavity leakage flow upstream of the subjected plane. Fig. 9b shows no influence on the distribution of isentropic efficiency from 30% to approximately 70% channel height with a constant value of $\eta_{is} \approx 95\%$. However, at the hub and the tip side the deviation increases. From the hub to approximately 30% channel height the deviation of η_{is} is nearly constant and equals $\Delta\eta_{is} \approx 2,5\%$. The difference in the surrounding area of the tip shows a way stronger deviation with a maximum of $\Delta\eta_{is} \approx 8\%$ at 80% channel height. This high loss is generated due to the ingress of entropy by the rotor cavity (② in Fig. 8). In total, the decay of the averaged isentropic efficiency caused by the cavity leakage is $\Delta\eta_{is} \approx 2,5\%$.

TIME AVERAGED RESULTS

Previous analysis of loss generation and secondary flow formation have been carried out based on steady state simulations using a mixing plane approach to achieve inter-row coupling, accepting the mentioned disadvantages. To extend the scope of application of the described effects to transient calculations, unsteady computations have been conducted. To account for the movement of the rotor relative to the stator, a zonal approach is used. Thus, a flow field as it actually develops within an axial turbine is simulated and interaction between rows like potential field and wake are reproduced. In order to give a brief overview of the results and differences to the steady state simulation, the time averaged transient results will be discussed in this section. To specify regions of loss generation due to cavity flow, the circumferentially and mass flow averaged isentropic efficiency of the first stage is evaluated in Fig. 10a as a function of the channel height. The depicted distribution reveals three significant areas. The first ① is defined by the highest discrepancy between both simulations starting from the shroud down to approximately 95% channel height. In agreement with the deviation in flow direction, this appears to be due to the mixing losses caused by the increased shearing between main and cavity flow. The second region ② can be found between 30% and 95% channel height. This area does not seem to be affected by the leakage ingress and is slightly bigger than in the steady state prediction. The third area ③ beneath 30% channel height confirms the enhanced development of secondary flow in the upstream rows, resulting in a decay of efficiency compared to the simulation without cavities. In total, the decay of the averaged efficiency caused by the cavity leakage is $\Delta\eta_{is} \approx 2,55\%$ and is therefore negligibly higher compared to the steady-state calculations. The flow field behind the second stator of the investigated turbine is evaluated by the distribution of mass flow weighted and circumferentially averaged total pressure as depicted in Fig. 10b. Compared to the simulation excluding cavities, the area indicated by ④ reveals the existence of an enhanced passage vortex in the simulation with cavities starting from the shroud down to 70% channel height, what resembles

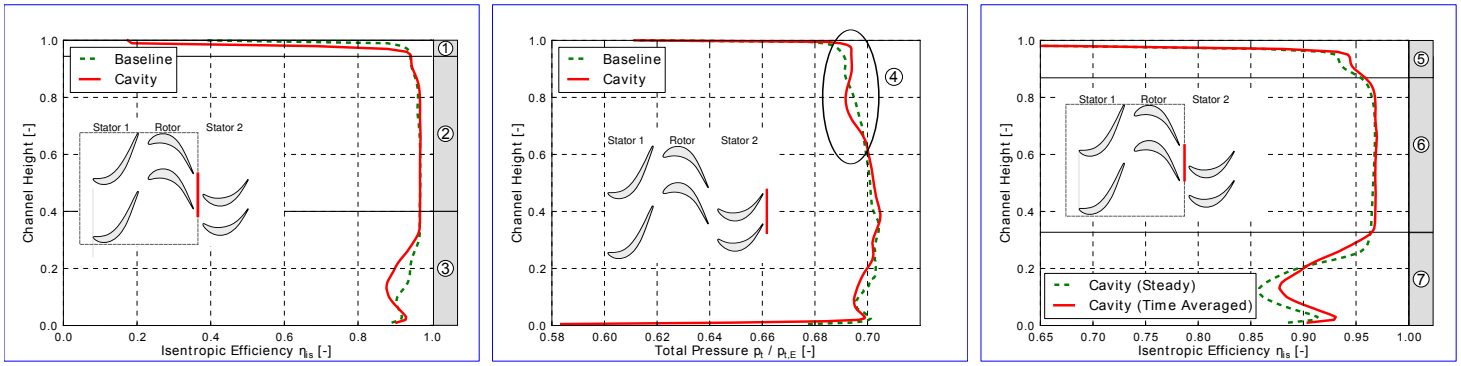

(a) (b) (c)

FIGURE 10: CIRCUMFERENTIALLY AVERAGED DISTRIBUTION OF: (a) ISENTROPIC EFFICIENCY OF FIRST STAGE, (b) TOTAL PRESSURE BEHIND SECOND STATOR, (c) ISENTROPIC EFFICIENCY OF FIRST STAGE FOR TRANSIENT AND STEADY CALCULATIONS

the corresponding prediction made by the steady state computation. As a result of the displacement caused by the enhanced secondary-flow structures, a slightly increased total pressure can be found in the midspan region from 40% to 60% channel height.

In order to verify the assumptions that are made when using a mixing plane approach, Fig. 10c shows the pitch-wise averaged total-to-total isentropic efficiency of the first stage for the transient and steady calculation with cavities. There are several regions which can be separated for evaluation. First region indicated as ⑤ in Fig. 10c reveals that losses in the vicinity of the tip down to approximately 90% span slightly differ. The steady-state calculation predicts significantly more losses in this area. The second region, starting from 80% down to 30% span and marked as ⑥ in Fig. 10c, shows agreement for both analysis. The third region, indicated as ⑦, reveals a significant difference between both pattern in the vicinity of the hub up to 30% span. This finding underscores the need for further investigation concerning the formation of unsteady vortex structures within the main flow caused by cavity leakage ingress.

TIME RESOLVED RESULTS

In the following section an extensive analysis of the influence on vortex formation will be given with an emphasis on the cavity outlet of the first stator. The pressure distribution near the cavity outlet is mostly affected by the flow field given by the first stator row. By definition, in the proximity of the suction side the pressure is lower than near the pressure side. This pressure field is superimposed by the potential field induced by the rotor. The range of influence of the latter is strongly limited to the leading edge of the rotor blades. As a result, the pressure field is subject to fluctuations which correlate with the RPM and the

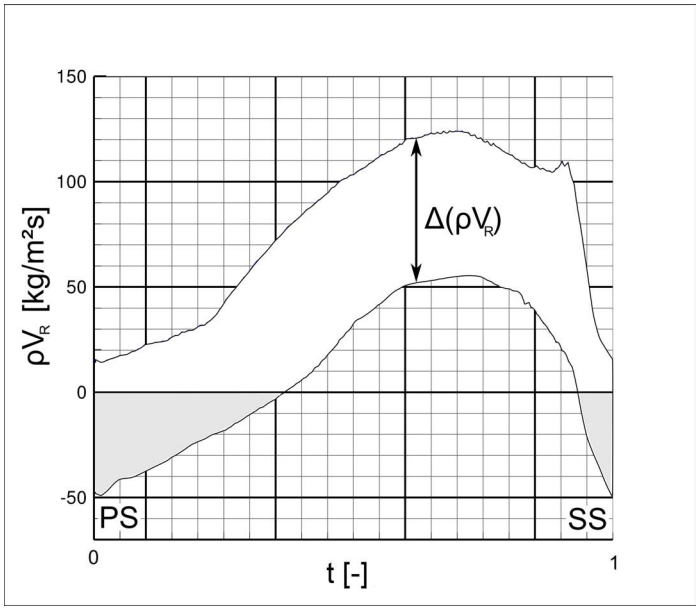

FIGURE 11: DENSITY FLUX OUT OF THE FIRST STATOR CAVITY OUTLET DRAWN OVER ONE PITCH OF THE FIRST STATOR. THE BLOCKAGE OF THE PASSING ROTOR LEADS TO FLUCTUATIONS WITH A MAGNITUDE OF $\Delta(\rho V_R)$; THE EXACT VALUE OF FLUX IS WITHIN THE ENVELOPE AREA

number of rotor blades. As described by Anker and Mayer [14] and Pfau et al. [1], the mass flux at the outlet of the cavity depends on the pressure field and corresponding flow resistance. Therefore, a fluctuation of the leakage flow can be expected. The distribution of density flux at the cavity outlet as a function of

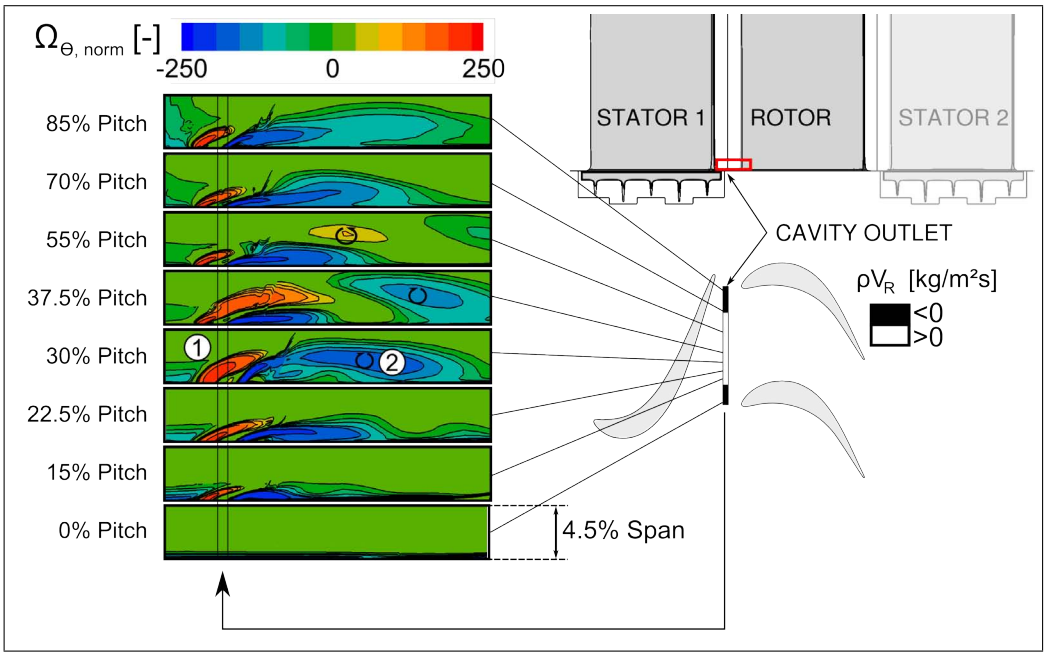

FIGURE 12: VORTEX FORMATION IN THE VICINITY OF THE CAVITY'S OUTLET

the first stator pitch is shown in Fig. 11. Due to the blockage caused by the downstream blade, the exact amount of density flux depends on the position of the rotor blade. Therefore, every possible amount that can be achieved is within the envelope area depicted in Fig. 11. Except for a small region, the magnitude of the flux-fluctuation $\Delta(\rho V_R)$ remains constant. In the area close to the trailing edge, cavity leakage reaches a local minimum. If the rotor passes this region, the pressure gradient inverts. As a consequence, the density flux inverts as well. Thus, mass flow is pushed back into the cavity. As a result of the described behavior, the subsequent blade rows are exposed to a fluctuating jet.

To obtain an overview of the influence of the oscillating leakage jet on the formation of flow structures in terms of vortices, the circumferential component of the vorticity Ω_Θ normalized with the rotor blade passing frequency is evaluated. Figure 12 shows the distribution of the circumferential vorticity Ω_Θ for different meridional slices in the region of the leakage flow. Additionally, a meridional- and blade to blade view of the turbine is given, indicating the position of observation within the turbine. The declaration of the pitch in Fig. 12 refers to the rotor. Within the wake of the first stator row, indicated as 0% pitch in Fig. 12, the influence of the potential field of the rotor leads to a slight suction of fluid into the cavity. Moving in direction of rotation, the cavity leakage flow increases. In the upstream region of the cavity exit, this causes the formation of a corner vortex (red, ① in Fig. 12) and a separation bubble downstream of the cavity (blue, ② in Fig. 12). Hence, the leakage flow acts as an obstacle within the main flow. Furthermore, as depicted at 37.5% and 50% pitch, mentioned vortices are torn away by the main flow. Towards the suction side of the first stator, the leakage flow decreases due to the blockage of the rotor and thus also the cause for the vortex formation and resulting vortices.

CONCLUSIONS

In order to investigate the interaction of cavity leakage flow and main flow, three dimensional steady-state and time-resolved RANS computations of a 1.5 stage axial turbine with and without labyrinth seals have been performed.

To obtain a thorough understanding of how the (inevitable) labyrinth leakage flow affects the formation of secondary flow and losses, comparisons of simulations with completely spatially discretized labyrinth seals and a smooth end wall have been conducted. Generally speaking, steady state and time resolved predictions show a good agreement with regard to the secondary flow effects. However, in a detailed analysis, differences can be observed, leading to the assumption that unsteadiness affects the flow field and loss formation. Nevertheless, the influence of the cavity leakage ingress is limited to the hub and tip. In the midspan region of the turbine almost no effect is observed. Due to the difference in tangential momentum, the leakage flow causes major losses when re-entering the main flow. Labyrinth leakage enhances the formation of vortices; primarily the passage vortex is affected. Transient simulations reveal that the mass flux at the cavity exit is non-uniform and subject to fluctuations caused by the movement of the downstream blade row and

accompanying blockage, resulting in a backflow of free stream fluid into the cavity. A detailed analysis of the region of leakage ingress is conducted and reveals that the leakage flow acts as an obstacle within the main flow, causing the development of a pair of counter-rotating vortices. In combination with the leakage flux fluctuation mentioned above, another time dependent effect is induced. The present investigation shows the need for further study regarding the interaction of the counter rotating pair of vortices with the surrounding secondary flow. Furthermore, mixing losses and losses generated within the cavity have not been separated.

ACKNOWLEDGMENTS

The authors gratefully acknowledge the substantial contributions of the DLR Institute of Propulsion Technology and MTU Aero Engines. Additionally, the authors thank MTU Aero Engines for the permission to publish this work and the North-German Supercomputing Alliance (HLRN) for the provided computational resources. The results presented in this paper have been obtained for research conducted with the *4th Aeronautical Research Program* of the German Ministry of Economics.

REFERENCES

[1] Pfau, A., Kalfas, A. I., and Abhari, R. S., 2007. "Making use of labyrinth interaction flow". *Journal of Turbomachinery,* ***129***(1), pp. 164–174.

[2] Denton, J. D., and Johnson, C. G., 1976. An Experimental Study of the Tip Leackage Flow Around Shrouded Turbine Blades. Technical report, Marchwood Engineering Laboratories. CEGB Report No. R/M/N848.

[3] Denton, J. D., 1993. "Loss mechanism in turbomachines". *Journal of Turbomachinery,* ***115***, pp. 621–656.

[4] Wallis, A. M., Denton, J. D., and Demargne, A. A. J., 2001. "The control of shroud leakage flows to reduce aerodynamic losses in a low aspect ratio, shrouded axial flow turbine". *Journal of Turbomachinery,* ***123***(2), pp. 334–341.

[5] Rosic, B., and Denton, J. D., 2008. "Control of shroud leakage loss by reducing circumferential mixing". *Journal of Turbomachinery,* ***130***(2), p. 021010.

[6] Gier, J., Stubert, B., Brouillet, B., and de Vito, L., 2005. "Interaction of shroud leakage flow and main flow in a three-stage lp turbine". *Journal of Turbomachinery,* ***127***(4), pp. 649–658.

[7] Anker, J. E., and Mayer, J. F., 2002. "Simulation of the interaction of labyrinth seal leakage flow and main flow in an axial turbine". *ASME Conference Proceedings,* ***2002***(3610X), pp. 217–224.

[8] Hunter, A. D., and Manwaring, S. R., 2000. "Endwall cavity flow effects on gaspath aerodynamics in an axial flow turbine: Part 1 experimental and numerical investigation". In ASME Turbo Expo, 2000-GT-651.

[9] Bolestis, E., Sieverding, C. H., and van Hove, W., 1983. "Effects of a skewed inlet end wall boundary layer on the 3d flow field in an annular turbine cascade". In AGARD Conference Proceedings, Vol. 351, pp. 16.1–16.16.

[10] Walsh, J. A., and Gregory-Smith, D., 1989. "Inlet skew and the growth of secondary losses and vorticity in a turbine cascade". In ASME Turbo Expo. 89-GT-65.

[11] Bindon, J. P., 1980. "Exit plane and suction surface flows in an annular turbine cascade with a skewed inlet boundary layer". *Journal of Heat and Fluid Flow,* ***2***, pp. 57–66.

[12] Pfau, A., Treiber, M., Sell, M., and Gyarmathy, G., 2001. "Flow interaction from the exit cavity of an axial turbine blade row labyrinth seal". *Journal of Turbomachinery,* ***123***(2), pp. 342–352.

[13] Pfau, A., Schlienger, J., Rusch, D., Kalfas, A. I., and Abhari, R. S., 2005. "Unsteady flow interactions within the inlet cavity of a turbine rotor tip labyrinth seal". *Journal of Turbomachinery,* ***127***(4), pp. 679–688.

[14] Anker, J. E., Mayer, J. F., and Casey, M. V., 2005. "The impact of rotor labyrinth seal leakage flow on the loss generation in an axial turbine". *Proceedings of the Institution of Mechanical Engineers, Part A: Journal of Power and Energy,* ***219***(6/2005), pp. 481–490.

[15] Wilcox, D. C., 1998. *Turbulence Modeling for CFD*, 2nd ed. DCW Industries, Inc.

[16] Kožulović, D., Röber, T. K., Kügeler, E., and Nürnberger, D., 2004. "Modifications of a two-equation turbulence model for turbomachinery fluid flows".

[17] Wilcox, D. C., 1992. "The remarkable ability of turbulence model equations to describe transition". In The Fifth Symposium on Numerical and Physical Aspects of Aerodynamic Flows, California State Univ., DCW Industries, Inc.

[18] Kožulović, D., Röber, T., and Nürnberger, D. "Application of a multimode transition model to turbomachinery flows". *Proceedings of the 7th European Turbomachinery Conference, Athens*.

[19] Yang, H., Nuernberger, D., Nicke, E., and Weber, A., 2003. "Numerical investigation of casing treatment mechanisms with a conservative mixed-cell approach". *ASME Conference Proceedings,* ***2003***(36894), pp. 961–974.

[20] Kügeler, E., Nürnberger, D., Weber, A., and Engel, K., 2008. "Influence of blade fillets on the performance of a 15 stage gas turbine compressor". *ASME Conference Proceedings,* ***2008***(43161), pp. 415–424.